Applied Catalysis B: Environmental 163 (2015) 129–134

Contents lists available at ScienceDirect

Applied Catalysis B: Environmental

journal homepage: www.elsevier.com/locate/apcatb

Full Length Article

The highest catalytic activity in the hydrolysis of ammonia borane by poly(*N*-vinyl-2-pyrrolidone)-protected palladium–rhodium nanoparticles for hydrogen generation

Murat Rakap*

Maritime Faculty, Yuzuncu Yil University, 65080, Van, Turkey

ARTICLE INFO

Article history:
Received 16 June 2014
Received in revised form 12 July 2014
Accepted 25 July 2014
Available online 2 August 2014

Keywords:
Palladium
Rhodium
Nanoparticle
Ammonia borane
Hydrogen

ABSTRACT

The use of poly(*N*-vinyl-2-pyrrolidone)-protected palladium–rhodium nanoparticles (2.5 ± 1.1 nm) as highly efficient catalysts providing a record catalytic activity in the hydrolysis of ammonia borane for hydrogen generation is reported. They are prepared by co-reduction of palladium and rhodium metal ions in ethanol/water mixture by an alcohol reduction method and characterized by TEM-EDX analysis, UV–Vis spectroscopy, and X-ray photoelectron spectroscopy. They are recyclable and highly efficient catalysts for hydrogen generation from the hydrolysis of ammonia borane even at very low concentrations and temperature, providing record average turnover frequency (1333 mol H_2 (mol cat)$^{-1}$ min^{-1}), maximum hydrogen generation rate (36,414 L H_2 min^{-1} (mol cat)$^{-1}$), and total turnovers (171,000). Poly(*N*-vinyl-2-pyrrolidone)-protected palladium-rhodium nanoparticles also provide activation energy of 46.1 ± 2 kJ/mol for the hydrolysis of ammonia borane.

1. Introduction

Ammonia borane (H_3NBH_3, AB) has recently been employed as a solid hydrogen storage material due to its high hydrogen content (19.6 wt%), high solubility and stability in water at room temperature [1,2]. AB is able to release hydrogen upon hydrolysis at room temperature in the presence of suitable catalysts according to Eq. (1):

$$H_3NBH_3(aq) + 2H_2O(l) \xrightarrow{catalyst} NH_4^+(aq) + BO_2^-(aq) + 3H_2(g) \quad (1)$$

Various kinds of catalyst systems have been tested for the hydrolysis of AB so far. Among those, nanoparticle-types were mostly employed catalysts, providing good catalytic activities as expected due to the small particle sizes. Some examples of those are hollow Ni-SiO_2 nanosphere [3], Fe(0) NPs [4], Co(0) NCs [5], polymer-stabilized Ru(0) and Pd(0) NCs [6], Co(0) NPs [7], water/air-stable Ni NPs [8], hollow Co-B nanospindles [9], nanoparticle-assembled Co-B thin film [10], Cu/Co_3O_4 NPs [11], SiO_2 supported monodisperse Ni NPs [12], Co-SiO_2 nanosphere [13], graphene oxide supported Pd NPs [14], Ru NPs [15], HAP-supported Co(0) [16], HAP-supported Pd(0) [17], Pd(0) NPs on $CoFe_2O_4$ [18], and HAP-supported Ru(0) [19].

However, the addition of second element to the monometallic nanoparticles will definitely improve the catalytic properties. Therefore, the employment of highly active bimetallic-type nanoparticles as catalyst for hydrogen generation from the hydrolysis of AB has recently been focused and some bimetallic nanoparticle-type catalysts including Ni@Ru core–shell nanoparticles [20], Ni-Ru alloy nanoparticles [21], RuCo and RuCu on γ-Al_2O_3 [22], RuCu on graphene [23], Ru@Ni core-shell nanoparticles [24], Cu-Ni on MCM-41 [25], Cu@FeCo core–shell nanoparticles [26], Ru@Co on graphene [27], and CoNi on graphene oxide [28] have been employed as catalysts. Additionally, recent articles related to use of poly(*N*-vinyl-2-pyrrolidone (PVP)-protected ruthenium–palladium [29] and platinum–ruthenium [30] nanoparticles showed that they are highly efficient catalysts for hydrogen generation from boron compounds providing remarkable results. However, there is no reported work on the catalytic activity of PVP-protected palladium-rhodium (Pd-Rh@PVP) nanoparticles in hydrogen production from the hydrolysis of AB, to the knowledge. This study reports the employment of Pd-Rh@PVP nanoparticles as highly efficient catalyst for hydrogen generation from the hydrolysis of AB. The catalysts were prepared by an alcohol reduction method [31], found to be stable as colloidal dispersions, and characterized by transmission electron microscopy (TEM), X-ray photoelectron spectroscopy (XPS), and UV–Vis spectroscopy.

* Tel.: +90 432 225 17 01; fax: +90 432 486 54 13.
E-mail addresses: mrtrakap@gmail.com, muratrakap@gmail.com

http://dx.doi.org/10.1016/j.apcatb.2014.07.050
0926-3373/

Although the cost of noble metal catalysts is assumed to be high, the highest catalytic activity of the Pd-Rh@PVP nanoparticles makes them very promising candidates to be used as catalyst in developing efficient portable hydrogen generation systems using AB as solid hydrogen storage material since it would easily compensate the cost concerns.

2. Experimental

2.1. Materials

Potassium tetrachloropalladate (K_2PdCl_4), rhodium (III) chloride trihydrate ($RhCl_3{\cdot}3H_2O$), poly(*N*-vinyl-2-pyrrolidone) (PVP-40), and ammonia borane (H_3NBH_3) were purchased from Aldrich. Ethanol was purchased from Merck. Deionized water was distilled by water purification system (Milli Q-pure WS). All glassware and teflon coated magnetic stir bars were rinsed with acetone, followed by copious washing with distilled water before drying in an oven at 150 °C.

2.2. Preparation of Pd-Rh@PVP nanoparticles

Pd-Rh@PVP nanoparticles were prepared by an alcohol reduction method in which PVP serves as both stabilizer and reducing agent. First, solutions of potassium tetrachloropalladate (0.25 mmol in 25 mL ethanol) and rhodium (III) chloride trihydrate (0.25 mmol in 25 mL water) were mixed and poly(*N*-vinyl-2-pyrrolidone) (PVP-40, 2.5 mmol of monomeric units) was added to this solution. Then, the mixed solution was refluxed at 90 °C for 2 h. Pd-Rh@PVP nanoparticles are brownish black in color and stable at room temperature. The total concentration of both metals was kept as 5.0 mM in 50 mL of the mixed solution.

2.3. Characterization of Pd-Rh@PVP nanoparticles

Transmission Electron Microscopy analysis was carried out using a JEOL-2010 microscope operating at 200 kV, fitted with a LaB_6 filament and has lattice and theoretical point resolutions of 0.14 nm and 0.23 nm, respectively. Samples were examined at magnification between 100 and 400 K. One drop of dilute suspension of sample was deposited on the TEM grids and the solvent was then evaporated. The diameter of each particle was determined from the enlarged photographs. X-ray photoelectron spectrum of the nanoparticles was taken by using SPECS spectrometer equipped with a hemispherical analyzer and using monochromatic Mg-Kα radiation (1250 eV, the X-ray tube working at 15 kV and 350 W). UV–Vis spectra were recorded on a Cary 5000 (Varian) UV–Vis spectrophotometer. A quartz cell with a part length of 1 cm was used and spectra were collected over the range of 200–900 nm. ^{11}B NMR spectra were recorded on a Bruker Avance DPX 400 with an operating frequency of 128.15 MHz for ^{11}B. D_2O and $BF_3{\cdot}(C_2H_5)_2O$ were used as a lock and external reference, respectively. At the end of the hydrolysis reaction, the resulting solutions were filtered and the filtrates used for taking ^{11}B NMR spectra.

2.4. Catalytic evaluation of Pd-Rh@PVP nanoparticles in the hydrolysis of AB

The catalytic activity of Pd-Rh@PVP nanoparticles in the hydrolysis of AB in aqueous solution was determined by measuring the rate of hydrogen generation. In all the experiments, a jacketed reaction flask (50 mL) containing a Teflon-coated stir bar was placed on a magnetic stirrer (Heidolph MR-301) and thermostated to 25.0 ± 0.1 °C by circulating water through its jacket from a constant temperature bath. Then, a graduated glass tube (50 cm in height and 4.0 cm in diameter) filled with water was connected to the reaction flask to measure the volume of the hydrogen gas to be evolved from the reaction. In a typical experiment, 63.6 mg (2 mmol) of H_3NBH_3 was dissolved in 20 mL of water. The solution was transferred with a glass pipet into the reaction flask thermostated at 25.0 ± 0.1 °C. Then, aliquots of Pd-Rh@PVP nanoparticles from the stock solution (5.0 mM) were added into the reaction flask. The experiment was started by closing the flask and the volume of hydrogen gas evolved was measured by recording the displacement of water level at the stirring speed of 1000 rpm. In addition to the volumetric measurement of the hydrogen evolution, the conversion of AB ($\delta = -23.9$ ppm) [32] to metaborate ($\delta = 9$ ppm) [33] was also checked by ^{11}B NMR spectroscopy.

2.5. The effect of stirring speed on hydrogen generation rate

The same experiment described in the Section 2.4 for the hydrogen generation from the hydrolysis of AB was performed at 25 ± 0.1 °C by varying the stirring speed (0, 200, 400, 600, 800, 1000, and 1200 rpm) to check how hydrogen generation rate from the hydrolysis of AB system was affected by stirring speed. The hydrogen generation rate was found to be independent of the stirring speed when it is higher than 800 rpm. This indicates that the system is in a non-mass transfer limitation regime since the present kinetic study was performed at the stirring speed of 1000 rpm.

2.6. The effect of PVP concentration on the catalytic activity of Pd-Rh@PVP nanoparticles in the hydrolysis of AB

In order to study the effect of PVP concentration on the catalytic activity of Pd-Rh@PVP nanoparticles in the hydrolysis of AB (100 mM), hydrolysis reactions were conducted in the presence of catalysts prepared with different [PVP/Cat.] ratios (2, 4, 6, 8, 10, 12, 14, 16). All the experiments were conducted in the same way described in Section 2.4. The optimum [PVP/Cat.] ratio was found to be 10. When this ratio is lower than 10, the catalytic activity of the catalyst is relatively low because PVP molecules do not cover the surface of nanoparticles effectively, leading to decreased catalytic activity by not preventing the agglomeration of nanoparticles. When it is higher than 10, catalytic activity of the catalyst starts to decrease since the surface of the nanoparticles may be wholly covered by PVP, blocking the active sites to be reached by substrate molecules. Therefore, optimum [PVP/Cat.] ratio was determined as 10 for further kinetic studies.

2.7. Determination of activation energy of Pd-Rh@PVP nanoparticles in the hydrolysis of AB

In a typical experiment, the hydrolysis of AB (100 mM) catalyzed by Pd-Rh@PVP nanoparticles (0.3 mM) was performed by following the same procedure described in Section 2.4 at various temperatures (5, 10, 15, 20, and 25 °C) to obtain the activation energy (E_a).

2.8. Determination of catalytic lifetime of Pd-Rh@PVP nanoparticles in the hydrolysis of AB

Catalytic lifetime of Pd-Rh@PVP nanoparticles in the hydrolysis of AB was determined by measuring the total turnover number (TTON). Such a lifetime experiment was started with a 20 mL aqueous solution containing Pd-Rh@PVP nanoparticles (0.3 mM) and H_3NBH_3 (600 mM) at 25.0 ± 0.1 °C. Once complete conversion is achieved, another equivalent of H_3NBH_3 was added and

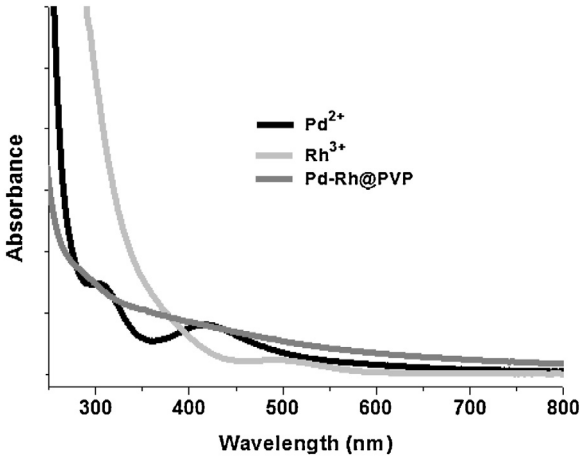

Fig. 1. UV–Vis absorption spectra of the aqueous solutions of K_2PdCl_4, $RhCl_3{\cdot}3H_2O$, and Pd-Rh@PVP nanoparticles.

the reaction was continued until no hydrogen gas evolution was observed.

2.9. Recyclability of Pd-Rh@PVP nanoparticles in the hydrolysis of AB

The recyclability of Pd-Rh@PVP nanoparticles in the hydrolysis of AB was determined by a series of experiments started with a 20 mL solution containing 0.3 mM Pd-Rh@PVP nanoparticles and 100 mM AB at 25.0 ± 0.1 °C. When the complete conversion is achieved, another equivalent of AB was added to the reaction mixture immediately. The results were expressed as % initial catalytic activity of Pd-Rh@PVP nanoparticles versus the number of catalytic runs in the hydrolysis of AB solution.

3. Results and discussion

3.1. Preparation and characterization of Pd-Rh@PVP nanoparticles

Pd-Rh@PVP nanoparticles were prepared from the co-reduction of mixture of potassium tetrachloropalladate and rhodium (III) chloride trihydrate by an alcohol reduction method in the presence of PVP in ethanol-water mixture at refluxing temperature. PVP serves as stabilizer and reducing agent. After refluxing for 2 h, the color of the solution turned to brownish black, indicating reduction of Pd^{2+} and Rh^{3+} ions to Pd^0 and Rh^0 to form bimetallic nanoparticles of them. Monitoring the UV–Vis electronic absorption spectra of the solution provides the best way to follow this conversion. Fig. 1 shows the spectral change during the formation of Pd-Rh nanoparticles from the reduction of corresponding palladium and rhodium salts by PVP. The absorption bands due to d–d transitions in Pd^{2+} and Rh^{3+} ions completely disappear after refluxing the solution, indicating the complete reduction of corresponding ions.

The size, morphology and composition of Pd-Rh@PVP nanoparticles were investigated by TEM-EDX analyses. Fig. 2 shows the TEM image taken at 50 nm magnification (Fig. 2a) and the corresponding EDX spectrum (Fig. 2c) of Pd-Rh@PVP nanoparticles, confirming 1:1 alloy structure which was also confirmed by ICP analysis. The mean particle size was determined as 2.5 ± 1.1 nm from TEM image by counting 212 non-touching particles.

Fig. 3 shows the survey scan (Fig. 3a) XPS spectrum of Pd-Rh@PVP nanoparticles and high resolution XPS spectra of Pd 3d (Fig. 3b) and Rh 3d (Fig. 3c) regions. Pd 3d region shows two peaks observed at 336.6 eV for $3d_{5/2}$ and 341.7 eV for $3d_{3/2}$, confirming the presence of Pd(0) [34]. Similarly, Rh 3d region also shows two peaks observed at 308.2 eV for $3d_{5/2}$ and 312.9 eV for $3d_{3/2}$, confirming the presence of Rh(0) [35]. There were some shifts (1.9 eV) to the higher binding energies stem from the increase of electron

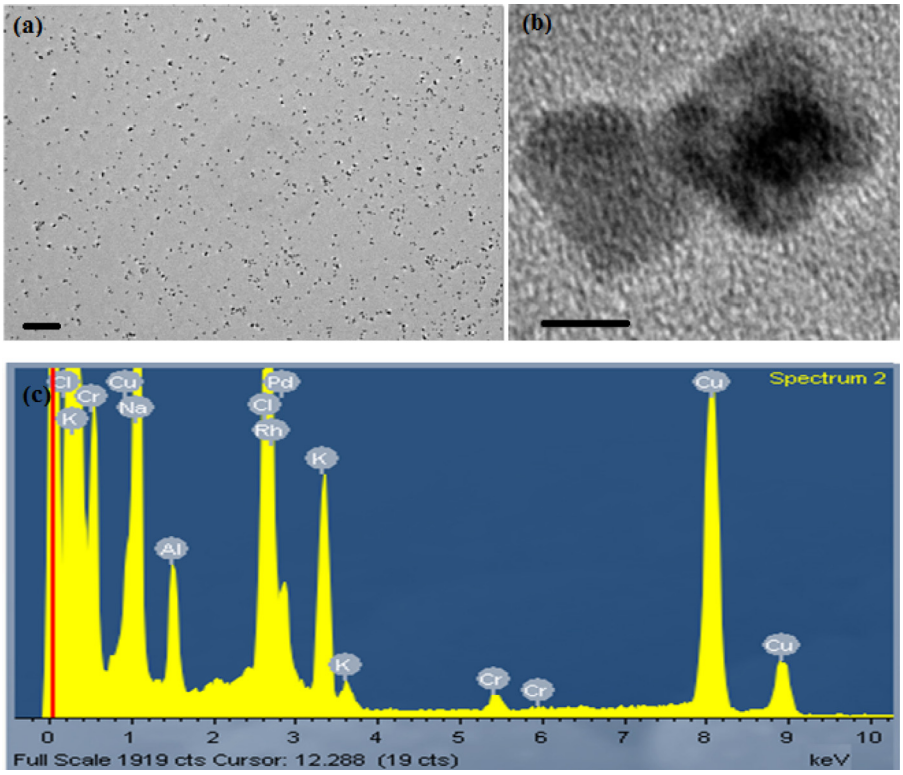

Fig. 2. TEM images taken at different magnifications (a) 50 nm and (b)100 nm after 5th use in hydrolysis reaction) and (c) the corresponding EDX spectrum of Pd-Rh@PVP nanoparticles.

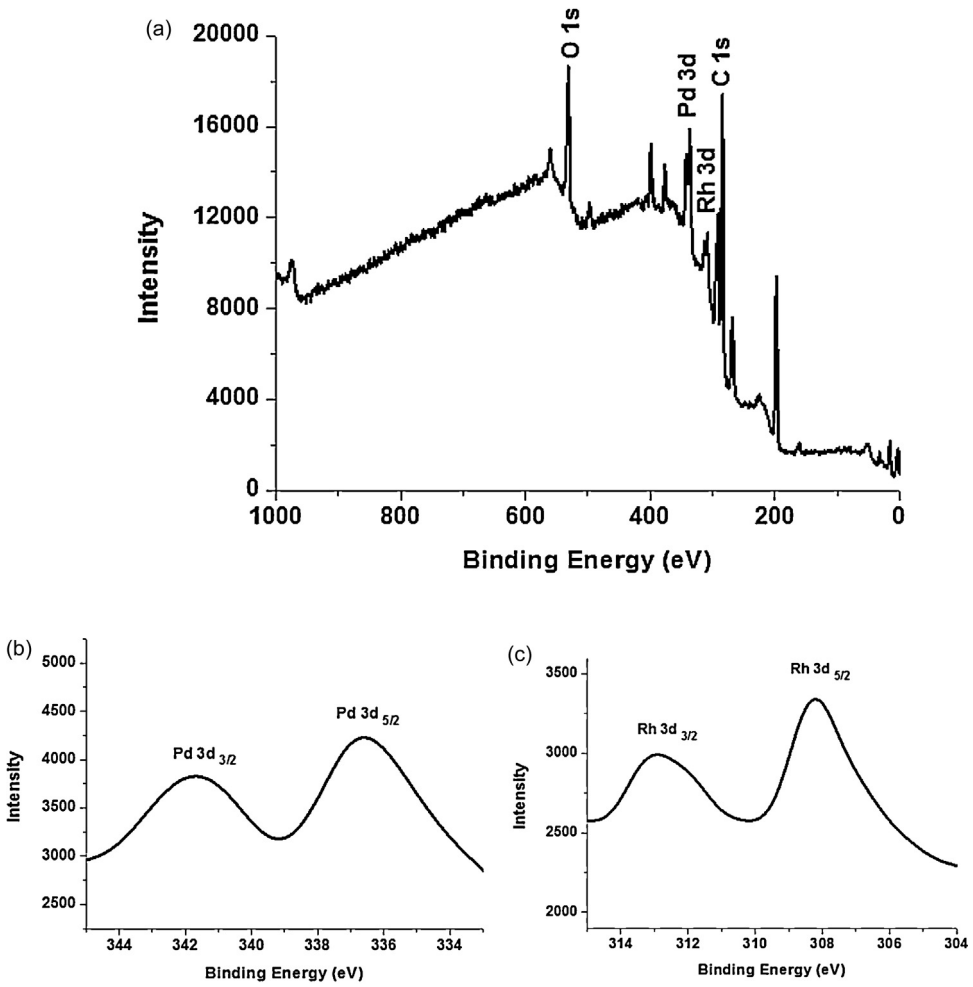

Fig. 3. (a) Survey scan X-Ray photoelectron spectrum of Pd-Rh@PVP nanoparticles with high resolution spectrum of (b) Pd 3d and (c) Rh 3d regions.

densities around metal atoms in the bimetallic nanoparticles due to the interaction between palladium and rhodium. There is no higher oxidation state peak for both metals of the catalyst in the XPS spectra, indicating the protection of Pd(0) and Rh(0) species by the attachment of PVP during catalyst preparation procedure.

Additionally, the formation of alloy type Pd-Rh@PVP nanoparticles rather than the physical mixtures of individual monometallic nanoparticles was confirmed by the comparison of the catalytic activities of all the types (monometallic Pd and Rh nanoparticles, 1:1 physical mixture of them, and 1:1 Pd-Rh bimetallic nanoparticles) in the hydrolysis of AB. They provided following turnover frequency (TOF) values in terms of mol H_2 mol catalyst^{-1} min^{-1}: 182 for Pd@PVP nanoparticles, 228 for Rh@PVP nanoparticles, 430 for 1:1 physical mixture of Pd@PVP and Rh@PVP nanoparticles, and 1333 for Pd-Rh@PVP bimetallic nanoparticles. Since Pd-Rh@PVP nanoparticles provided a much higher catalytic activity than the physical mixture of Pd and Rh monometallic nanoparticles, it was clearly understood that the prepared catalyst is composed of alloy type Pd-Rh@PVP bimetallic nanoparticles rather than a mixture of the individual monometallic nanoparticles. This much higher catalytic activity of bimetallic nanoparticles stems from the synergistic effects of palladium and rhodium [36].

3.2. Catalytic evaluation of Pd-Rh@PVP nanoparticles in the hydrolysis of AB

Pd-Rh@PVP nanoparticles were found to be highly efficient catalysts for the hydrolysis of AB. Fig. 4 shows the plots of mol H_2/mol AB versus time in the catalytic hydrolysis of 100 mM AB solutions in the presence of Pd-Rh@PVP nanoparticles in different catalyst concentrations (0.1, 0.2, 0.3, 0.4, and 0.5 mM) at 25.0 ± 0.1 °C. The linear hydrogen generation starts immediately without an induction period and continues until the complete hydrolysis of AB. Moreover, the control tests using copper(II) sulfate trap with acid–base

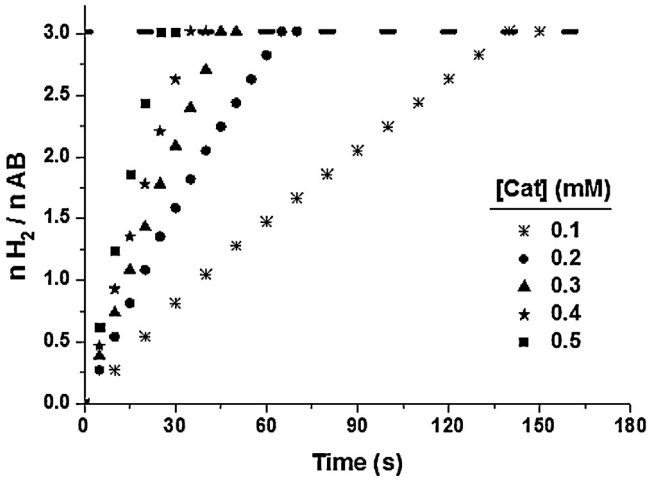

Fig. 4. Plot of mol H_2/mol AB versus time for the hydrolysis of 100 mM AB solutions in the presence of Pd-Rh@PVP nanoparticles in different catalyst concentrations (0.1, 0.2, 0.3, 0.4, and 0.5 mM) at 25.0 ±0.1 °C.

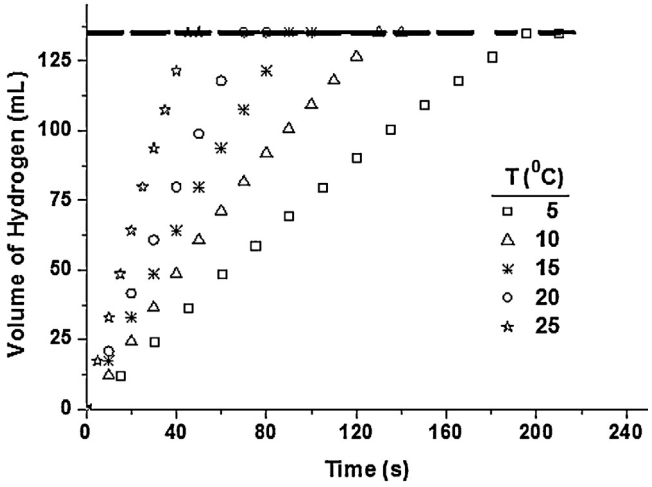

Fig. 5. Plots of the volume of generated hydrogen gas versus time in the catalytic hydrolysis of 100 mM AB solutions in the presence of Pd-Rh@PVP nanoparticles (0.3 mM) at various temperatures (5, 10, 15, 20, and 25 °C).

Table 1
Activities in terms of TOF values of various catalyst systems tested in hydrogen generation from the hydrolysis of AB (The TOF values were either directly taken or estimated from the data given in respective references.).

Catalyst	TOF (mol H_2 mol catalyst^{-1} min^{-1})	Reference
Pd-Rh@PVP NPs	1333.0	[This Study]
Ru-Pt@PVP NPs	308.0	[30]
Ru-Pd@PVP NPs	308.0	[29]
Laurate-stabilized Rh(0) NCs	200.0	[35]
Zeolite-Rh(0) NCs	92.0	[43]
Co	44.2	[7]
In-situ Co(0) NPs	39.8	[2]
RGO-Pd NPs	26.3	[14]

indicators resulted in no ammonia evolution in detectable amount in the experiments conducted in this study. Additionally, conversion of AB ($\delta = -23.9$ ppm) to metaborate ($\delta = 9$ ppm) was also checked by ^{11}B NMR spectroscopy.

Fig. 5 shows the plots of the volume of generated hydrogen gas versus time in the catalytic hydrolysis of 100 mM AB solutions in the presence of Pd-Rh@PVP nanoparticles (0.3 mM) at various temperatures (5, 10, 15, 20, and 25 °C). It is worth to note that using Pd-Rh@PVP nanoparticles (0.3 mM) leads to complete hydrogen release (3.0 mol H_2/mol AB) for the hydrolysis of AB within 45 s, corresponding to a record average TOF value of 1333 mol H_2 (mol cat)$^{-1}$ min^{-1} at 25.0 ± 0.1 °C. This record TOF value is 4.32 times higher than the previous values of 308 for Ru-Pt@PVP nanoparticles [30] and Ru-Pd@PVP nanoparticles [29]. The much higher catalytic activity of Pd-Rh@PVP nanoparticles stems from the synergistic effects of palladium and rhodium and the reduced particle size of the catalyst. TOF values of various catalysts in the hydrolysis of AB are given in Table 1, for comparison.

The rate constants of hydrogen generation from the hydrolysis of AB were calculated from the linear portions of the plots given in Fig. 5 at five different temperatures and used for the calculation of the activation energy (E_a = 46.1 ± 2 kJ/mol for the hydrolysis of AB) from the Arrhenius plot (Fig. 6) for hydrolysis reaction. This activation energy of 46.1 ± 2 kJ/mol for the hydrolysis of AB is lower than the activation energies reported in the literature for the same reaction using many different catalysts: 70 kJ/mol for bulk nickel [37], 63 kJ/mol for PVP-stabilized cobalt(0) nanoclusters [38], 56 kJ/mol for zeolite confined palladium(0) nanoclusters [34], 52 kJ/mol for Ni-Ag/C [39], but still higher than 39 kJ/mol for $Pt_{0.65}Ni_{0.35}$ nanoparticles [40], 44 kJ/mol for PSSA-co-MA stabilized Pd(0) nanoclusters [6], 44 kJ/mol for (Co-Mo-B)/Ni foam [41], and 34 kJ/mol for SiO_2-supported monodisperse nickel nanoparticles [12].

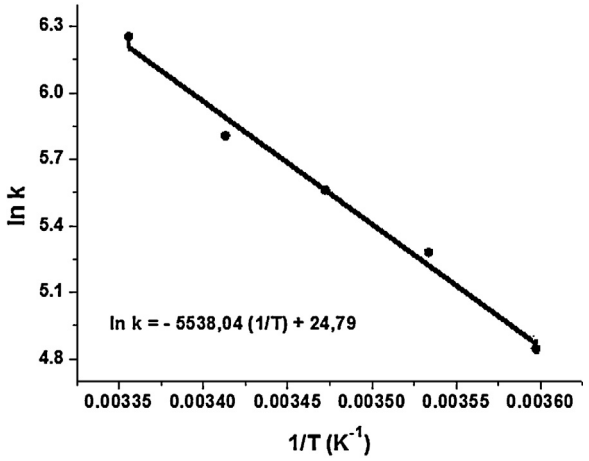

Fig. 6. Arrhenius plot for the hydrolysis of AB (100 mM) catalyzed by 0.3 mM Pd-Rh@PVP nanoparticles.

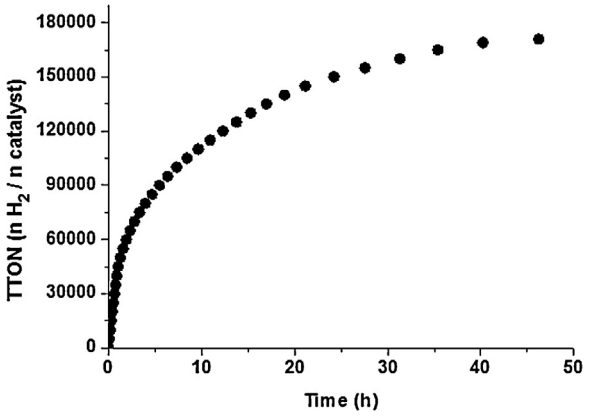

Fig. 7. Total turnover number (TTON) versus time (h) plot for hydrolysis of AB by Pd-Rh@PVP nanoparticles (0.3 mM) at 25.0 ± 0.1 °C.

3.3. *The recyclability and catalytic lifetime of Pd-Rh@PVP nanoparticles in the hydrolysis of AB*

The recyclability of Pd-Rh@PVP nanoparticles in the hydrolysis of AB was investigated by successive additions of AB after the first cycle of the hydrolysis reaction. The Pd-Rh@PVP nanoparticles catalyst retains 78% of its initial catalytic activity in the hydrolysis of AB, even at the fifth run. The slight decrease in the catalytic activity of Pd-Rh@PVP nanoparticles in the hydrolysis of AB is due to the passivation of nanoparticles' surface by increasing amount of metaborate, which decreases accessibility of active sites [42] and the aggregation of nanoparticles as shown in the TEM image of the catalyst taken after fifth run of the hydrolysis reaction (Fig. 2b, scale bar represents 100 nm) since there was no change in the composition of the catalyst after fifth run as determined by ICP analysis. More importantly, Pd-Rh@PVP nanoparticles provide 171,000 total turnovers over a period of 46 h before deactivation in the hydrolysis of AB at 25.0 ±0.1 °C (Fig. 7). This is a record total turnover value ahead of laurate-stabilized rhodium(0) nanoclusters (80,000) [35] and zeolite framework stabilized-rhodium(0) nanoclusters (47,200) [43].

4. Conclusions

In summary, the study of the preparation, characterization and employment of Pd-Rh@PVP nanoparticles as catalyst for the hydrolysis of AB has led to the following conclusions and insights:

- Pd-Rh@PVP nanoparticles can be easily prepared from the co-reduction of corresponding palladium and rhodium salts by an alcohol reduction method.
- Pd-Rh@PVP nanoparticles are highly efficient catalyst for hydrogen generation from the hydrolysis of AB providing the best ever catalytic activity.
- They provide record average TOF (1,333 mol H_2 $(\text{mol cat})^{-1}$ min^{-1}), maximum hydrogen generation rate (36,414 L H_2 min^{-1} $(\text{mol cat})^{-1}$) and turnovers (171,000) for the hydrolysis of AB.
- Activation energy for the catalytic hydrolysis of AB in the presence of Pd-Rh@PVP nanoparticles was calculated as 46.1 ± 2 kJ/mol.
- Pd-Rh@PVP nanoparticles can be regarded as promising catalysts having highest activity for practical applications to supply hydrogen from the hydrolysis of AB for proton exchange membrane fuel cells.

Acknowledgement

This study is supported by Research Fund of Yuzuncu Yil University (Project No: BAP-2013-FEN-B-014).

References

[1] Q. Xu, M. Chandra, J. Power Sources 163 (2006) 364–370.
[2] T. Umegaki, J.M. Yan, X.B. Zhang, H. Shioyama, N. Kuriyama, Q. Xu, Int. J. Hydrogen Energ. 34 (2009) 3816–3822.
[3] T. Umegaki, J.M. Yan, X.B. Zhang, H. Shioyama, N. Kuriyama, Q. Xu, J. Power Sources 191 (2009) 209–216.
[4] J.M. Yan, X.B. Zhang, S. Han, H. Shioyama, Q. Xu, Angew. Chem. Int. Ed. 47 (2008) 2287–2289.
[5] R. Fernandes, N. Patel, A. Miotello, Appl. Catal. B: Environ. 92 (2009) 68–74.
[6] Ö. Metin, Ş. Şahin, S. Özkar, Int. J. Hydrogen Energ. 34 (2009) 6304–6313.
[7] J.M. Yan, X.B. Zhang, H. Shioyama, Q. Xu, J. Power Sources 195 (2010) 1091–1094.
[8] J.M. Yan, X.B. Zhang, S. Han, H. Shioyama, Q. Xu, Inorg. Chem. 48 (2009) 7389–7393.
[9] D.G. Tong, X.L. Zeng, W. Chu, D. Wang, P. Wu, J. Mater. Sci. 45 (2010) 2862–2867.
[10] N. Patel, R. Fernandes, G. Guella, A. Miotello, Appl. Catal. B: Environ. 95 (2010) 137–143.
[11] Y. Yamada, K. Yano, Q. Xu, S. Fukuzumi, J. Phys. Chem. C 114 (2010) 16456–16462.
[12] Ö. Metin, S. Özkar, S. Sun, Nano Res. 3 (2010) 676–684.
[13] T. Umegaki, J.M. Yan, X.B. Zhang, H. Shioyama, N. Kuriyama, Q. Xu, J. Power Sources 195 (2010) 8209–8214.
[14] B. Kılıç, S. Şencanlı, Ö. Metin, J. Mol. Cat. A: Chem. 361–362 (2012) 104–110.
[15] H. Can, Ö. Metin, Appl. Catal. B: Environ. 125 (2012) 304–310.
[16] M. Rakap, S. Özkar, Catal. Today 183 (2012) 17–25.
[17] M. Rakap, S. Özkar, Int. J. Hydrogen Energ. 36 (2011) 7019–7027.
[18] S. Akbayrak, M. Kaya, M. Volkan, S. Özkar, Appl. Catal. B: Environ. 147 (2014) 387–393.
[19] S. Akbayrak, P. Erdek, S. Özkar, Appl. Catal. B: Environ. 142–143 (2013) 187–195.
[20] G. Chen, S. Desinan, R. Nechache, R. Rosei, F. Rosei, D. Ma, Chem. Commun. 47 (2011) 6308–6310.
[21] G. Chen, S. Desinan, R. Rosei, F. Rosei, D. Ma, Chem. Eur. J. 18 (2012) 7925–7930.
[22] G.P. Rachiero, U.B. Demirci, P. Miele, Int. J. Hydrogen Energ. 36 (2011) 7051–7065.
[23] N. Cao, K. Hu, W. Luo, G. Cheng, J. Alloys Compd. 590 (2014) 241–246.
[24] N. Cao, J. Su, W. Luo, G. Cheng, Int. J. Hydrogen Energ. 39 (2014) 426–435.
[25] Z.H. Lu, J. Li, G. Feng, Q. Yao, Z.F. Zhang, R. Zhou, D. Tao, X. Chen, Z. Yu, Int. J. Hydrogen Energ. (2014), http://dx.doi.org/10.1016/j.ijhydene.2014.04.086.
[26] F. Qiu, Y. Dai, L. Li, C. Xu, Y. Huang, C. Chen, Y. Wang, L. Jiao, H. Yuan, Int. J. Hydrogen Energ. 39 (2014) 436–441.
[27] N. Cao, J. Su, W. Luo, G. Cheng, Catal. Commun. 43 (2014) 47–51.
[28] Y. Yang, F. Zhang, H. Wang, Q. Yao, X. Chen, Z.H. Lu, J. Nanomater. (2014), http://dx.doi.org/10.1155/2014/294350.
[29] M. Rakap, J Int. J. Green Energ. (2014), http://dx.doi.org/10.1080/15435075.2014.895737.
[30] M. Rakap, Appl. Catal. A: Gen. 478 (2014) 15–20.
[31] N. Toshima, M. Harada, T. Yonezawa, K. Kushihashi, K. Asakura, J. Phys. Chem. 95 (1991) 7448–7453.
[32] M. Chandra, Q. Xu, J. Power Sources 156 (2006) 190–194.
[33] K.S. Eom, K.W. Cho, H.S. Kwon, Int. J. Hydrogen Energ. 35 (2010) 181–186.
[34] M. Rakap, S. Özkar, Int. J. Hydrogen Energ. 35 (2010) 1305–1312.
[35] F. Durap, M. Zahmakıran, S. Özkar, Appl. Catal. A: Gen. 369 (2009) 53–59.
[36] H.L. Jiang, Q. Xu, J. Mater. Chem. 21 (2011) 13705–13725.
[37] S.B. Kalidindi, M. Indirani, B.R. Jagirdar, Inorg. Chem. 47 (2008) 7424–7429.
[38] Ö. Metin, S. Özkar, Energy Fuels 23 (2009) 3517–3526.
[39] C.F. Yao, L. Zhuang, Y.L. Cao, X.P. Hi, H.X. Yang, Int. J. Hydrogen Energ. 33 (2008) 2462–2467.
[40] X. Yang, F. Cheng, J. Liang, Z. Tao, J. Chen, Int. J. Hydrogen Energ. 34 (2009) 8785–8791.
[41] H.B. Dai, L.L. Gao, Y. Liang, X.D. Kang, P. Wang, J. Power Sources 195 (2010) 307–312.
[42] T.J. Clark, G.R. Whittell, I. Manners, Inorg. Chem. 46 (2007) 7522–7527.
[43] M. Zahmakıran, S. Özkar, Appl. Catal. B: Environ. 89 (2009) 104–110.